Profiles of flow discharged from vertical rotating pipes: A contrast between inviscid liquid and granular jets

P. D. Weidman,[1,a] J. P. Kubitschek,[1] and A. Medina[2]
[1]*Department of Mechanical Engineering, University of Colorado, Boulder, Colorado 80309, USA*
[2]*SEPI-ESIME-Azcapotzalco, IPN, Av. de las Granjas 682, Col. Sta. Catarina, Azcapotzalco C. P. 02550, Mexico Distrito Federal, Mexico*

(Received 8 May 2008; accepted 26 September 2008; published online 11 November 2008)

The stability of viscous rotating liquid columns and their application to rotating viscous liquid jets aligned under gravity is reviewed. Experiments on stable viscous fluid flow discharged from rotating vertical pipes exhibit very weak contraction. We present an elementary liquid jet analysis to understand this phenomenon. Indeed, our inviscid model of a slender rotating inviscid liquid jet shows that rotation suppresses contraction. Next we study the comparable problem for granular flow. Our model for noncohesive granular flow emanating from a vertical pipe rotating about its central axis, valid for sufficiently large rotation rate, shows that the granular profiles blossom rather than contract. The profiles of both the liquid and granular jets depend on the same dimensionless parameters—an exit Froude number Fr_0 and an exit swirl parameter χ_0. The limitations of both models are discussed. Experimental data for granular jet profiles compare well with the collision-free granular flow model in its range of applicability. A criterion for the rotation rate at which particles adjacent to the inner wall of the rotating pipe cease to flow is also given and compared to experiment. © *2008 American Institute of Physics*. [DOI: 10.1063/1.3013636]

I. INTRODUCTION

The nature and breakup of liquid jets have been under experimental and theoretical investigation since the time of Leonardo da Vinci. An extensive review of this work by Eggers and Villermaux,[1] with emphasis on surface tension effects, has recently become available in *Reports on Progress in Physics*. Another review focused on the break up of liquid jets and spray formation was given by Lin and Reitz[2] and more results may be found in the work of Middleman.[3]

While experimentally investigating the stability of rapidly rotating viscous liquid jets aligned with gravity,[4,5] the question arose regarding how stable rotating liquid jets contract. A photograph of a stable liquid jet emanating from a long rotating pipe is shown in Fig. 1(a). Our search of literature fails to locate any theoretical studies on the gravitational contraction of spinning liquid jets. However, a number of papers on the stability and break up of rotating liquid columns with application to rotating liquid jets are available; see the early study by Rutland and Jameson,[6] a very brief section in Eggers and Villermaux,[1] Eggers and Brenner,[7] and the recent work by Kubitschek and Weidman.[4,8] In the absence of rotation, a number of papers have been written on the shape of liquid jets leaving the orifice of straight pipes with and without the effect of gravity; see, for example, Middleman.[3]

To investigate the rather weak gravitational draw down apparent in Fig. 1(a), we consider the simplest model—that for an inviscid rotating liquid jet—which has the possibility of elucidating the effect of rotation on jet contraction. The remarkably simple and apparently new solution we obtain may be of more than pedagogical interest. Experiments with water jets emanating from a vertical pipe undergoing high rotation exhibit spectacular instabilities just downstream of the exit plane.[9] However, for certain flow rates in a carefully controlled experiment at low to moderate rotation rates, the *intact* length of a water jet is likely to extend many diameters downstream like that of a nonrotating water jet,[2] assuming stable flow within the rotating pipe. In either case, our solution provides a base flow for stability calculations of an inviscid liquid jet flow.

Granular gravity flow from pipes is an increasingly important topic of research due to its practical utility; see the books by Brown and Richards[10] and Duran[11] and the review article by Wieghardt.[12] Also, from a scientific point of view, the complex gravity flow that is observed to develop inside[13] and outside[14,15] of pipes offers interesting opportunities for modeling and analysis. In a general context, static[10,11,16] and a variety of dynamic[13–15,17] regimes of granular material and flow in vertical pipes is governed mainly by wall friction. For instance, in tall statically filled pipes and silos the pressure distribution along the downward axial coordinate from the free surface is initially hydrostatic, but saturates to a fixed value within 1–10 pipe diameters, depending on wall friction and properties of the granular material.[10,16] In gravitationally driven noncohesive granular flow down a vertical pipe, when the grains of diameter d are much smaller than the pipe of diameter D, dimensional analysis[10–12] reveals that the mean axial exit speed scales as $W \sim \sqrt{gD}$ and the mean volume flow rate scales as $Q \sim \sqrt{g}D^{5/2}$. Thus, for $d \ll D$ the grains play no fundamental role in this flow and for the experiments presented here $d/D=0.1$. When this criterion is not satisfied, one can still find adequate correlations of exit velocity and volume flow rate based on Beverloo's law with

[a]Electronic mail: weidman@colorado.edu.

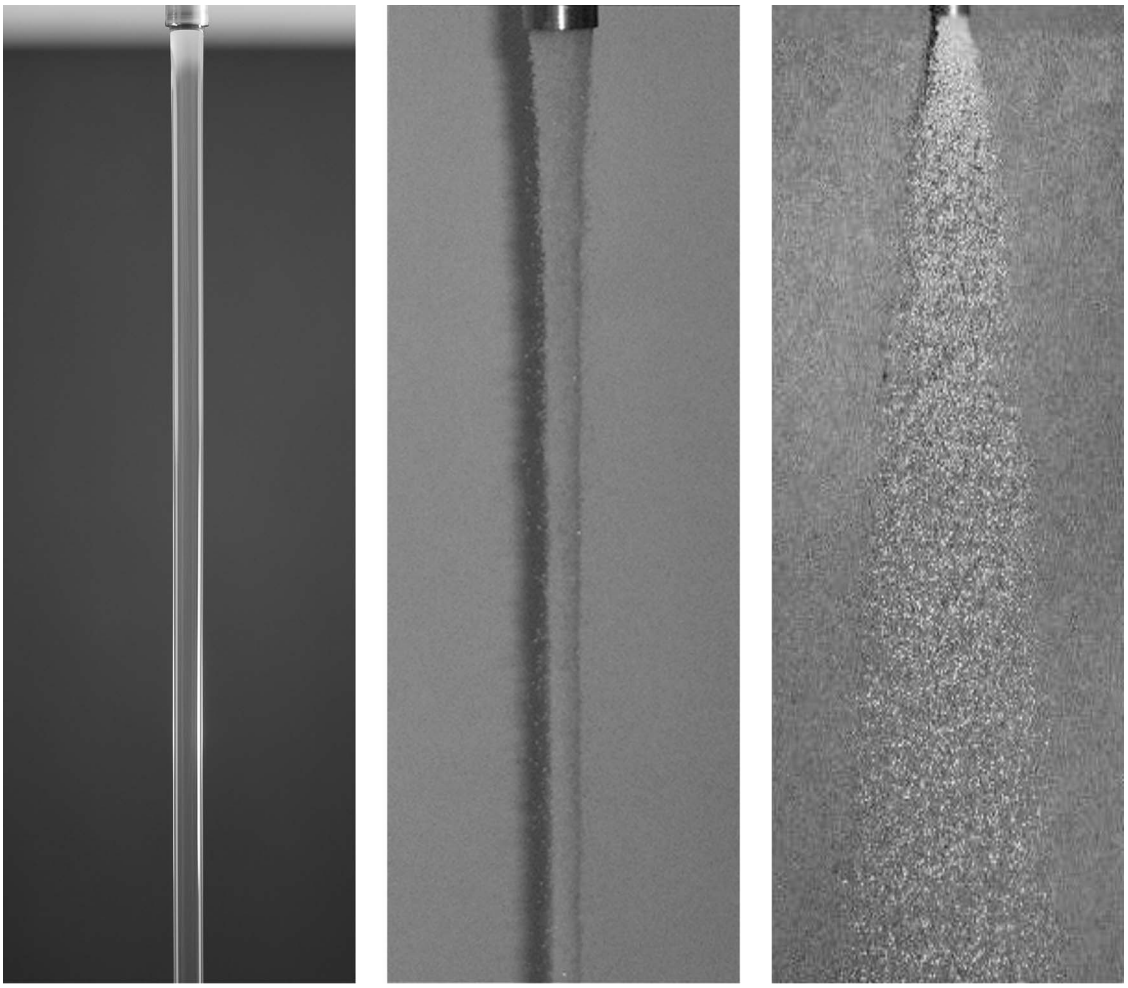

FIG. 1. Side view profiles of (a) a rotating viscous liquid jet: $R_0=0.35$ cm, $W_0=220$ cm/s, and $\Omega_0=104.7$ rad/s with visible jet length $h=13.5$ cm, (b) sand jet emanating from a stationary pipe: $R_0=0.50$ cm, $W_0=29.7$ cm/s, with visible jet length $h=16$ cm, and (c) sand jet emanating from a rotating pipe: $R_0=0.50$ cm, $W_0=10.0$ cm/s, and $\Omega_0=14.13$ rad/s with visible jet length $h=22$ cm.

one adjustable constant.[18] Recently, studies on how a granular jet maintains its own structure close to[15] and far from[14] the pipe orifice, or how it deforms under strong shocks,[15,19] have revealed that the behavior of granular jets sometimes resemble the behavior of liquid jets under similar circumstances, but other times the particulate nature of granular jet is imposed overwhelmingly.

The stationary granular jet shown in Fig. 2 of the study by Boudet *et al.*[15] on granular hydraulic jumps sparked our interest in granular jets formed at the exit of a rotating pipe. Photographs taken from our preliminary experimental setup show a noncohesive sand jet leaving a stationary pipe in Fig. 1(b) and one leaving a rotating pipe in Fig. 1(c). While the contracting granular profile in Fig. 1(b) resembles that of a liquid jet, the blossoming profile in Fig. 1(c) owes its existence to the particulate nature of the granular flow. It is important to note at the outset that what is observed in Fig. 1(c) is not a rotating granular jet, but simply a free jet formed as the gravity-driven granular flow is discharged from a vertical rotating pipe. Again, our search of literature has not revealed any study on the shape of this type of free granular jet.

To investigate this flow system, we consider the simplest granular model—that of collisionless granular projectile dynamics—which ought to elucidate the physics of expanding free granular jets. Measurements of free granular jet profiles afford a comparison with theoretical predictions and help ascertain the limits of the collision-free model. Solutions of our simplified models for the rotating liquid jet and the free granular jet show that both jet profiles are controlled by the same dimensionless parameters: an exit Froude number Fr_0 and an exit swirl parameter χ_0.

The presentation is as follows. The model for the shape of a rotating inviscid liquid jet and its associated pressure field is given in Sec. II. In Sec. III A a model for the shape of a collision-free granular jet formed at the exit of a vertical rotating pipe yields jet profiles which are compared to experiments presented in Sec. III B. Contrasting features of the two jets are discussed in Sec. IV, and the summary of results and concluding remarks are given in Sec. V.

II. INVISCID LIQUID JETS

For the assumed laminar axisymmetric inviscid flow, cylindrical coordinates (r,θ,z) with corresponding coordinate velocities (u,v,w) are employed. We choose z pointing downward aligned with gravity g.

Let us first recall the model often employed to determine the shape of a steady *nonrotating* inviscid jet. Incompressible liquid emanates with uniform axial velocity W_0 from the exit at $z=0$ of circular pipe of inner radius $r=R_0$. It is tacitly assumed that the axial velocity W is uniform over each downstream jet section and that surface tension, not accounted for in the mathematical model, is responsible for maintaining the axisymmetric stress-free boundary. Conservation of mass and application of Bernoulli's equation along a streamline on the constant pressure surface $r=R(z)$ of the jet, from the exit to arbitrary position z, furnish two equations involving the axial velocity and jet radius. Middleman[3] reported the jet profile in nondimensional form as

$$\frac{R}{R_0} = \left[1 + \mathrm{Fr}_0^{-1}\left(\frac{z}{R_0}\right)\right]^{-1/4}, \tag{1a}$$

where

$$\mathrm{Fr}_0 = \frac{W_0^2}{2gR_0} \tag{1b}$$

is the exit Froude number measuring the relative importance of inertial to gravitational forces. The pressure within the jet is everywhere equal to the atmospheric pressure p_a to which the jet is exposed. This result provides a basic understanding, for example, of the contraction of a smooth water jet leaving the faucet of a kitchen sink.

The effect of rotation on jet contraction may be obtained by continuation of the above simple model. We further assume the inviscid fluid leaves the orifice with uniform rotation rate Ω_0 and, like the axial velocity W, the axial vorticity 2Ω across each downstream section of the jet is uniform. Then the velocity vector on the surface $r=R(z)$ of the rotating liquid jet is

$$\mathbf{u} = \Omega R \mathbf{e}_\theta + W\mathbf{e}_z. \tag{2}$$

The absence of a radial velocity means we are dealing with a jet of slowly varying radius. Moreover, the jet radius R, its rotation rate Ω, and the axial velocity W all vary with downward coordinate z. Bernoulli's equation along streamlines

$$\frac{p}{\rho} - gz + \frac{U^2}{2} = C(\psi) \tag{3}$$

still holds for this steady inviscid vortical flow, although the Bernoulli constant now varies across the stream surfaces. Application of Eq. (3) along a spiral streamline on the constant pressure, stress-free surface $r=R(z)$ of the rotating liquid jet gives

$$U^2 = U_0^2 + 2gz, \tag{4a}$$

where U is the total velocity at downstream position z and U_0 is the total velocity at the pipe orifice, viz.,

$$U^2 = W^2 + (R\Omega)^2, \quad U_0^2 = W_0^2 + (R_0\Omega_0)^2. \tag{4b}$$

Conservation of mass requires

$$WR^2 = W_0R_0^2, \tag{5}$$

and Kelvin's theorem applies to this inviscid flow. Evaluation of the circulation around the exit circuit $r=R_0$ and a downstream circuit $r=R$ shows that angular momentum is conserved,

$$\Gamma = \oint \mathbf{u}\cdot\mathbf{dr} = 2\pi\Omega_0R_0^2 = 2\pi\Omega R^2. \tag{6}$$

Equations (5) and (6) are used to eliminate W and Ω in Bernoulli's Eq. (4). This gives a fourth order equation for the shape $R(z)$ of the swirling jet,

$$(W_0^2 + R_0^2\Omega_0^2 + 2gz)\left(\frac{R}{R_0}\right)^4 - (R_0\Omega_0)^2\left(\frac{R}{R_0}\right)^2 - W_0^2 = 0. \tag{7}$$

The physically relevant solution, written in dimensionless form, is

$$\frac{R}{R_0} = \sqrt{2}\left[\sqrt{(\chi_0^2+2)^2 + 4\mathrm{Fr}_0^{-1}\left(\frac{z}{R_0}\right)} - \chi_0^2\right]^{-1/2}, \tag{8a}$$

where χ_0 is the exit swirl parameter defined by

$$\chi_0 = \frac{R_0\Omega_0}{W_0}. \tag{8b}$$

When $\chi_0=0$, solution (1) for a nonrotating jet is recovered. In the opposite limit $\chi_0\to\infty$, taken holding Fr_0 fixed, one finds that the jet does not contract. Jet profiles for selected values of χ_0 are displayed in Fig. 2.

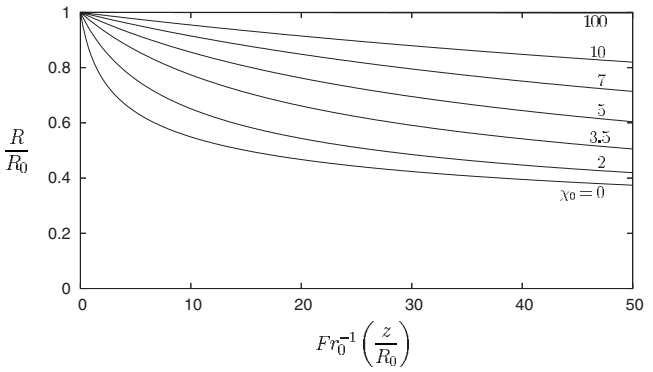

FIG. 2. Profiles for an inviscid rotating liquid jet for selected values of χ_0.

Equations (5) and (6) show that the local swirl parameter χ decreases in the same fashion as the jet radius, namely,

$$\chi(z) = \frac{R\Omega}{W} = \frac{\chi_0}{R_0}R(z). \tag{9}$$

Note that although the swirl parameter χ, proportional to R, decreases with z, the surface angular speed ΩR, proportional to R^{-1}, increases with z.

To complete the solution, the pressure within the jet must be determined from integration of the radial Euler equation

$$\frac{\partial p}{\partial r} = \rho\frac{(\Omega r)^2}{r}. \tag{10}$$

Solving for Ω in Eq. (6) permits integration of Eq. (10) from arbitrary radial position r to the jet surface R, where $p=p_a$. The result is

$$p(r,z) = p_a - \frac{\rho\Omega_0^2 R_0^2}{2}\left(\frac{R_0}{R}\right)^4\left[\left(\frac{R}{R_0}\right)^2 - \left(\frac{r}{R_0}\right)^2\right], \tag{11a}$$

where the z-dependent terms involving R/R_0 may be computed explicitly from Eq. (8a). Evaluation of Eq. (11a) at $r=0$ gives the axial variation of centerline pressure,

$$p(0,z) = p_a - \frac{\rho\Omega_0^2 R_0^4}{2R^2}. \tag{11b}$$

Clearly, viscosity and surface tension are neglected in this model. Middleman[3] reviewed the problem of laminar contraction of nonrotating viscous jets. For jets issuing from a horizontal tube at speeds for which its trajectory is unaffected by gravity over the dynamic range of interest, the classical momentum model showing the $0.866R_0$ contraction of in jet radius from a parabolic exit profile to a downstream plug flow is presented. Experiments show that such contraction is only achieved at large Reynolds number and that small Reynolds number jets expand rather than contract. Of the two important deficiencies in that momentum analysis, the neglect of axial vorticity that diffuses upstream to affect the velocity profile within the tube and the neglect of surface tension, Middleman noted that the latter was generally small compared to the former. In his review of models on the draw down of vertical viscous jets, the effect of surface tension is neglected altogether.

Our inviscid model for the contraction of rotating liquid jets does not suffer from the finite Reynolds number problem involving jet contraction adjustment of the viscous exit velocity profile; indeed the assumed exit velocity is already a spiraling plug flow. We expect that surface tension, particularly for the slender jet assumption inherent in the model, plays a secondary role in determining the contraction of the vertical rotating liquid jet over the intact region of laminar, stable flow. Of course, surface tension plays a fundamental role in determining the intact length of liquid jets, whether they rotate or not.[2] In any case, our mathematical description provides a rational explanation for why inviscid rotating jets contract more slowly than stationary jets. We return to this discussion in Sec. IV.

III. GRANULAR JETS

Our goal in this section is to provide an understanding of the basic characteristics of the free granular jet formed when the bottom exit of a vertical pipe, filled with a noncohesive granular material and undergoing rotation Ω_0 about its central axis, is suddenly opened. In this overall system, there are two flows: the inner confined flow and the external free flow. The internal flow is dominated by frictional and centrifugal forces. While at high rotation rates the external flow depends mainly on inertial and gravitational forces, as in Fig. 1(c), it is clear in Fig. 1(b) that at zero or low rotation rates the physics is complicated by interparticle momentum transfer and frictional energy losses. We anticipate, however, that when the pipe rotation is sufficiently large, the grains in the free jet will disperse with minimal collisions.

Experiments and a simple physical model allows one to conclude that an increase in Ω_0 provides, inside the pipe, an increase in wall friction with a corresponding decrease in volume flow rate. Moreover, at sufficiently high rotation, the internal flow may be arrested since gravity cannot overcome the ever increasing frictional force between the particulate matter and the wall. In the external free flow, pipe rotation induces, on the grains leaving the pipe, a tangential velocity that tends to increase the effective diameter of the free jet with a concomitant decrease in particle density.

Sections III A and III B provide a simple analytical model for the shape of a free granular jet discharged from a vertical rotating pipe, and a description of experiments conducted at the ESIME laboratory of the Instituto Politénico Nacional in Mexico City.

A. The model

Stable nonrotating gravity-driven granular jets of millimeter-sized glass beads exhibit contraction following the approximate law[15]

$$\frac{R}{R_0} \sim \left(\frac{z}{R_0}\right)^{-1/6}. \tag{12}$$

It is our understanding that a theoretical model for the shape of this granular jet has not yet been presented. It seems clear that contraction is caused by sidewall friction and particle collision for without either effect the particles would simply drop straight down under gravity forming, in the absence of aerodynamic drag, a cylindrical jet. Perhaps a higher velocity centerline stream entrains, through radial momentum transfer of interparticle collision, the slower moving grains near the cylindrical wall into a focused granular jet. Whatever the explanation may be, particle collisions are fundamental to the nature of the stationary free jet, and even for a slowly rotating pipe, the role of particle collisions must be taken into account. Once there is sufficient rotation, however, we expect the flow will be inherently collision-free and, in the absence of drag, will obey simple particle dynamics.

In view of the above discussion, we adopt a model based on the motion of a single grain (whose diameter is small compared to the tube radius) viewed from the inertial frame of the laboratory. Again, cylindrical coordinates (r,θ,z) with corresponding velocities (u,v,w) are employed and the following assumptions are adopted: (i) The particles at $z=0^-$ and $t=0^-$ are initially in rigid rotation Ω_0 about the z-axis and have uniform downward velocity W_0; (ii) aerodynamic drag is neglected; and (iii) the exit velocity conditions imply that grains initially at $r=r_0$, where $0\le r_0\le R_0$, move tangentially outward in collision-free motion with velocity $V_0 = r_0\Omega_0$ for $z=0^+$ and $t=0^+$.

A consequence of the above assumptions is that for $z>0^+$ and $t>0^+$ the particles are in frictionless projectile motion. We understand that the velocity at the exit of the tube will not be uniform, but we assume W_0 is uniform for simplicity. In fact, it is easy to anticipate that the side view profile of the free jet will depend only on those particles leaving the orifice from the inner rim of the rotating pipe. The single governing equation of motion for each particle is

$$\ddot{z} = g, \tag{13}$$

giving

$$z = W_0 t + \tfrac{1}{2} g t^2, \tag{14}$$

with solution

$$t = \frac{1}{g}(\sqrt{W_0^2 + 2gz} - W_0). \tag{15}$$

The trajectory of a particle depends on the initial position (r_0, θ) at which it leaves the horizontal exit plane. Parametrizing the location of the particle with time t, its absolute position relative to its departure point is given by

$$\mathbf{r} - r_0 \mathbf{e}_r = (r_0 \Omega_0 t)\mathbf{e}_\theta + z(t)\mathbf{e}_z. \tag{16}$$

The motions of individual particles leaving the inner rim $r_0 = R_0$ of the cylinder are in $\mathbf{r} = R_0 \mathbf{e}_r$ planes which rotate with θ. To be specific, let the rotating unit vector $\mathbf{e}_r(\theta)$ be instantaneously aligned, at $\theta = 0$, with the x-axis of an inertial Cartesian reference system (x, y, z). Then the coordinates in a horizontal plane perpendicular to the jet are given by $x = r \cos\theta$ and $y = r \sin\theta$. For $\theta = 0$ the motion of a single particle leaving the inner wall will have a trajectory parallel to the inertial y-z plane. The profile for this single particle, denoted here as $S(z)$, is determined by the $\mathbf{e}_\theta$-component of Eq. (16) and insertion of the parameter t given in Eq. (15) yields

$$S(z) = \frac{\Omega_0 R_0}{g}\left(\sqrt{W_0^2 + 2gz} - W_0\right). \tag{17}$$

The profile $R(z)$ of the free granular jet is the envelope of all trajectories [Eq. (17)] projected onto the y-z plane as they are produced from various points (R_0, θ) around the inner exit rim of the rotating tube. Particles leaving from points $R_0 \sin\theta$ have trajectory projections $S(z)\cos\theta$; thus, the jet profile is the envelope of trajectories given by

$$y(z) = R_0 \sin\theta + S(z)\cos\theta. \tag{18}$$

The envelope over the range $0 \le \theta \le \pi/2$ will provide the right-half side view profile $R(z)$ which is, of course, axisymmetric about the z-axis. Following the standard procedure for determining the envelope of curves with a parameter, we differentiate Eq. (18) with respect to θ to obtain

$$S(z) = R_0 \cot\theta. \tag{19}$$

Inserting Eq. (19) into Eq. (18) gives

$$y = R_0 \csc\theta, \tag{20}$$

which is used to calculate

$$\cot\theta = \frac{\sqrt{y^2 - R_0^2}}{R_0}. \tag{21}$$

The parameter θ is now eliminated by inserting Eq. (21) into Eq. (19) and solving for envelope profile $y(z) \equiv R(z)$, which gives

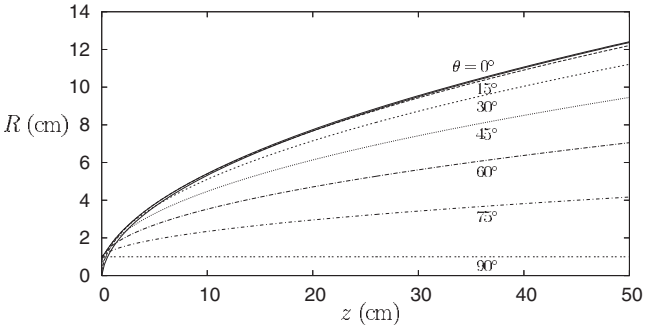

FIG. 3. Projection onto the y-z plane of particle trajectories leaving the inner rim of the rotating pipe at selected angles θ computed using Eq. (18). The envelope of trajectories $R(z)$ calculated from Eq. (22) is shown as the solid line.

$$R(z) = \sqrt{R_0^2 + S^2(z)} = R_0 \sqrt{1 + \frac{\Omega_0^2}{g^2}(\sqrt{W_0^2 + 2gz} - W_0)^2}. \tag{22}$$

A plot of individual trajectories $y(z)$ computed from Eq. (18) for selected values of θ is given in Fig. 3 along with its envelope $R(z)$ computed from Eq. (22) plotted as the dark solid line. We see that the envelope profile near the exit of the tube is defined by those particles leaving near $\theta = 90°$ while the asymptotic shape of the profile as $z \to \infty$ is defined by the particles leaving near $\theta = 0°$.

In nondimensional form the granular jet profile may be written as

$$\frac{R}{R_0} = \sqrt{1 + 4\chi_0^2 \mathrm{Fr}_0^2\left(\sqrt{1 + \mathrm{Fr}_0^{-1}\left(\frac{z}{R_0}\right)} - 1\right)^2} \tag{23}$$

where Fr_0 and χ_0 are defined in Eqs. (1b) and (8b), respectively.

Sample dimensionless profiles of a blossoming jet, computed at $\mathrm{Fr}_0 = 0.1$ are displayed in Fig. 4 at selected values of χ_0. With increasing χ_0, the particles discharged from the inner rim of the tube tend toward a horizontal trajectory before descending as an umbrella under the influence of gravity. Note also that the deflection of the jet with respect to the z-axis at the exit is zero. Further discussion of these latter two points will be given in Sec. IV.

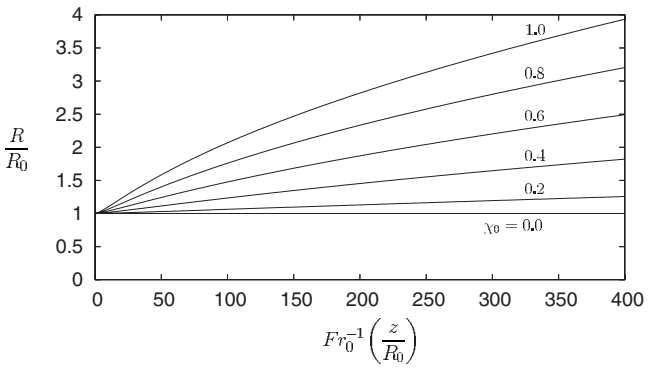

FIG. 4. Profiles for the granular jet at $\mathrm{Fr}_0 = 0.1$ for selected values of χ_0.

B. An Experiment

Our first setup consisting of a plastic tube supported by two fixed rotary bearings suffered from electrostatic effects in the 30%–35% humidity laboratory environment. Moreover, small tube vibrations were observed during rotation owing to the long distance between the support bearings. Both deficiencies were overcome in our second apparatus comprised of a thin walled steel pipe vertically aligned and secured by three fixed bearings located at the middle, upper, and lower ends of the pipe. The pipe was fitted at its upper part to the shaft of a high-torque motor controlled by an ac power supply. Pipe rotation rate was recorded by a digital tachometer. A grounded metal wire wrapped several times around the pipe, in a slip-fit fashion, provided continuous electrostatic discharge. No significant vibration of the pipe during rotation was observed.

A unique protocol was followed to produce the granular jets. First the pipe of measured inner radius $R_0 = 0.500 \pm 0.001$ cm and length $L=90$ cm was filled with near monodisperse 1 mm diameter Ottawa sand and tapped to attain the initial static height $H=80$ cm. The tapping procedure was considered the best method for producing near-identical column packings for each experiment. Small 1 mm holes piercing the top sidewall of the pipe vented the air pocket above the sand to the ambient pressure. After 1 min of rotation at the desired angular velocity, a small cardboard stopper at the exit was removed to initiate the gravity flow.

This same protocol was employed to determine the average volume flow rate Q as a function of pipe rotation rate Ω_0. The flow rate was obtained by measurement of the time T to collect a volume V of grains in a Pyrex measuring cup. The cup intercepting the granular stream just below the exit a short time after inception was removed before complete evacuation in an attempt to eliminate the high and low flow rates that occur, respectively, at the beginning and end of the discharge.[10] Large 80 cm^3 volumes were collected at low rotation rates with fast discharge, while smaller volumes down to 20 cm^3 were collected at the highest rotation rates where extremely slow discharge was observed. Note that these are naturally collected uncompacted volumes in contrast to the compacted volumes initially in the pipe.

From the average value of Q obtained using repeated measurements at each rotation rate, the average exit velocity $W_0 = Q/\pi R_0^2$ was calculated. The results plotted in Fig. 5 have W_0 error bars determined through propagation of time ($\delta t = \pm 0.1$ s), volume ($\delta V/V = \pm 0.05$), and radius ($\delta R = \pm 0.001$ cm) measurement errors. The error bars in Ω_0 due to tachometer accuracy ($\delta\Omega = \pm 10$ rpm) are buried within the size of the plotting symbols.

Three distinct regimes are apparent in Fig. 5. Region I ($0 < \Omega_0 < 76$ rad/s) exhibiting a slow attenuation of W_0 is followed by a rather sharp transition ($76 < \Omega_0 < 92$ rad/s) to extremely low values of W_0, which mark the beginning of region II ($92 < \Omega_0 < 157$ rad/s). All flows to the end ($\Omega \simeq 92$ rad/s) of the transition region were observed to be continuous, whereas the flow in region II is characterized by discretely ejected particles. The end point of region II plotted as the solid circle is the rotation rate where, finally, no particles leave the pipe, ostensibly due to particle jamming along the centerline near the exit. Linear least-squares fits of the data plotted as solid lines in Fig. 5 give a slope −0.0360 cm/rad in region I and a much smaller slope −0.00455 cm/rad in region II.

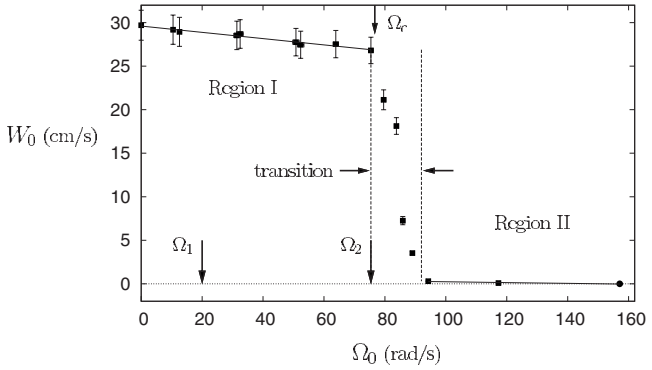

FIG. 5. Variation of measured mean axial velocity W_0 with pipe rotation rate Ω_0 showing regions I and II connected by a narrow transition. The arrows marking $\Omega_1 = 20$ rad/s and $\Omega_2 \simeq 76$ rad/s represent our best estimates for the onset of collisionless flow, and the end of continuum flow, respectively. The arrow marking $\Omega_c = 76.7$ rad/s represents the onset of the transition region calculated from Eq. (25).

The streak photographs displayed in Fig. 6 for $\Omega_0 = 11.9$, 23.0, and 51.6 rad/s were used to measure the jet profiles in region I. Four duplicates of each photograph in Fig. 6 were printed on A4 paper on which the image of the inner tube diameter (1.000 cm) was measured with a micrometer to ±0.01 mm. Neglecting minor parallax errors, this sets the scale factor and accuracy for subsequent measurement of the jet diameters which are determined from the width of the bright white region in each image. The systematic linear error was typically 2.9%. Repeated measurements of each jet diameter at fixed, uniformly spaced axial positions were used to compute the mean jet radius and its estimated uncertainty based on the Student-t distribution with $\nu = 3$ at a 95% confidence level. The final error bars for R/R_0 were computed as the root mean square of the systematic linear error and the Student-t uncertainty. The uncertainty in z/R_0 is simply the systematic linear error.

The measured jet profiles R/R_0 plotted as a function of axial position z/R_0 in Fig. 7 for each value of χ_0 are compared to theoretical predictions given by Eq. (23) shown as solid lines. The values of W_0 used to calculate χ_0 and Fr_0 are determined from region I linear fit in Fig. 5, and their uncertainties calculated through propagation of error are given in Fig. 7. Recall that we have implicitly assumed the particles at the rim of the tube leave the pipe with the average axial velocity W_0. Indeed the axial velocity may not be uniform across the exit plane, but we have not endeavored to measure the exit velocity profile and take this possible nonuniformity into account in this preliminary model. Note that the theoretical curves depend weakly on Fr_0 since W_0 varies less than 5% over the region $12 < \Omega_0 < 52$ rad/s of data collection.

The first thing to recognize in Fig. 7 is that the experimental data at $\chi_0 = 0.404$ and $\chi_0 = 0.799$ agree within 95% confidence level with results from the simple model. At $\chi_0 = 0.206$, however, the data fall consistently below the theo-

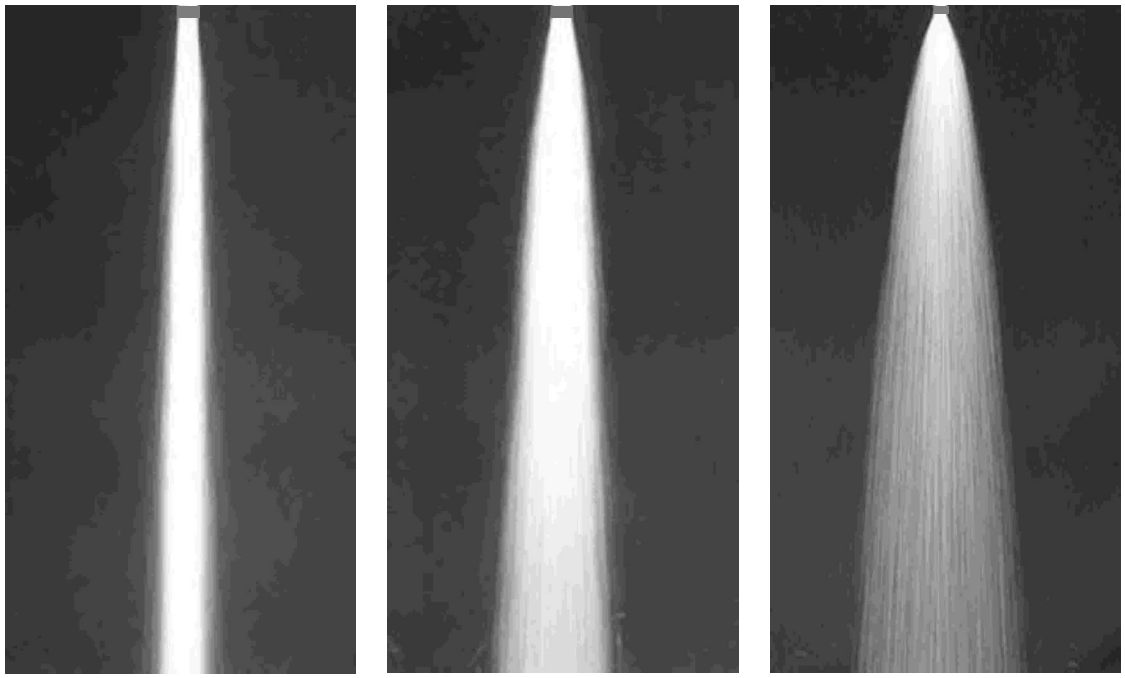

FIG. 6. Streakline photographs of the granular flow; (a) $\mathrm{Fr}_0=29.17$ and $\chi_0=0.206$, (b) $\mathrm{Fr}_0=28.79$ and $\chi_0=0.404$, and (c) $\mathrm{Fr}_0=27.73$ and $\chi_0=0.799$. The vertical field of view is approximately $h=40$ cm.

retical prediction. We ascribe this discrepancy to residual particle interactions for this slowly rotating pipe; evidently the transition to inherently collision-free particle motion takes place somewhere between $\chi_0=0.206$ and $\chi_0=0.404$. Thus the transition is somewhere between 11.9 and 23.0 rad/s and, for lack of more refined data, we estimate this transition to be at $\Omega_1 \simeq 20$ rad/s. Since the theoretical model assumes continuous and collision-free particle motion, we are now able to establish, for this experimental setup, the approximate range of validity $\Omega_1 < \Omega_0 < \Omega_2$ for the values Ω_1 and Ω_2 plotted in Fig. 5.

Now we turn to the problem of modeling the sudden decrease in volume flow rate, i.e., how the granular flow at the wall is first arrested. The flow was induced when the lower outlet of the spinning pipe was opened. At this instant of incipient free fall, the pressure in the zone of height $h \simeq R_0$ close to the exit drops to zero.[10,12] In this zone the averaged frictional force acts opposite to the weight. The normal force is here assumed to be composed of the integrated centrifugal force and the horizontal projection of the weight of the particles onto the sidewall moderated by the Janssen constant. Thus, the balance of forces is achieved when

$$\pi R_0^3 \rho g = \mu_w \left(\frac{2\pi\rho\Omega_0^2 R_0^4}{3} + 2\pi R_0^3 K \rho g \right), \tag{24}$$

where ρ is the bulk density of the granular medium, μ_w is the wall friction coefficient, and K is the Janssen constant characterizing the conversion of vertical into horizontal stress due to the imbricated nature of the granulate which takes values such that in many practical cases, the product $\mu_w K$ is of the order 0.1.[10] From Eq. (24), it is possible to obtain the critical angular velocity Ω_c for which the particles at the inner wall of the pipe will be arrested, viz.,

$$\Omega_c = \sqrt{\frac{3g(1-2\mu_w K)}{2\mu_w R_0}}. \tag{25}$$

To check the validity of this prediction, we have experimentally determined that $\mu_w=0.4$ for the Ottawa sand used in our experiments and take $\mu_w K=0.1$. This gives the critical angular velocity $\Omega_c=76.7$ rad/s. Note that the particles just inside the annulus of arrested particles experience a smaller normal centrifugal force, and can thus continue sliding down the pipe until, at still higher rotation rate, they are arrested. Of course, the dynamics of the particle flow in this transition

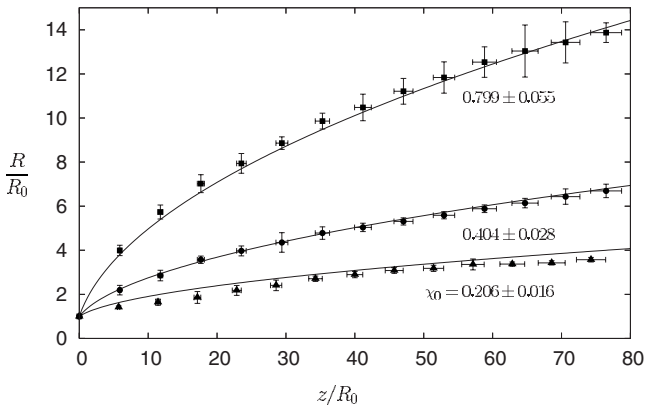

FIG. 7. Granular jet profiles at the three indicated values of χ_0 with measurements in solid symbols and theoretical results from Eq. (22) marked by the solid lines; $\mathrm{Fr}_0=29.17\pm0.099$ (triangles), $\mathrm{Fr}_0=28.79\pm0.097$ (circles), and $\mathrm{Fr}_0=27.73\pm0.088$ (squares).

region is very complex, and beyond our simple modeling capability.

It is possible to gain more physical understanding of the quantity Ω_c if we rearrange the terms in Eq. (25) into the critical rotational Froude number,

$$\mathrm{Fr}_c = \frac{\Omega_c^2 R_0}{g} = \frac{3(1-2\mu_w K)}{2\mu_w}, \tag{26}$$

representing the ratio of centrifugal to gravitational forces. Introduction of the above values for μ_w and K into Eq. (26) yields the estimate $\mathrm{Fr}_c \simeq 3$. Again, the granular nature of the sand is imposed on the solid-like behavior that is assumed in the model given by Eqs. (24)–(26). During rotation, the grains very close to the center of the pipe experience a very small centrifugal force, even if Ω_0 is large. The granular jet profiles expand with increasing Ω_0, but when $\Omega_0 > \Omega_c$ the integrity of the jet is compromised; particles near the wall are arrested and at higher rotation rates particles at smaller radii also get arrested until, in region II, individual grains, apparently discharged from the bottom center of the rotating granular bulk, are intermittently expelled from the pipe.

IV. CONTRASTING FEATURES OF THE JETS

The basic effect of rotation on the jet profiles is clear. With increasing pipe rotation Ω_0 the inviscid liquid jet contracts more slowly than a stationary jet while its density remains constant, the liquid being held in place by surface tension. At low rotation, the granular jet contracts less rapidly than the 1/6th power-law contraction observed by Boudet *et al.*[15] for a stationary granular jet until a condition of no contraction ($R \simeq R_0$) is reached; with further increase in Ω_0, the granular jet expands with ever decreasing particle density.

Now having rudimentary models for the shape of liquid and granular jets emanating from vertical rotating pipes under the influence of gravity, we are in a position to make direct comparisons of their behavior. Of particular interest are the near-exit and far-field behaviors of the jets. First, we calculate the asymptotic jet profiles at large axial distance z. Using Eq. (8a), one finds the asymptotic shape of the contracting inviscid liquid jet,

$$R \sim R_0^{5/4}\mathrm{Fr}_0^{1/4} z^{-1/4}, \quad z \to \infty, \tag{27}$$

and from Eq. (23) the asymptotic shape of the expanding granular jet is

$$R \sim 2\chi_0 (R_0 \mathrm{Fr}_0)^{1/2} z^{1/2}, \quad z \to \infty. \tag{28}$$

It is interesting that the limiting rotating liquid jet profile given by Eq. (27) is independent of the swirl parameter, and therefore must be identical to that of a nonrotating inviscid liquid jet, as may be verified from Eq. (1). The asymptotic shape of the granular jet, on the other hand, depends on both χ_0 and Fr_0.

Next we compare the angles with respect to vertical at which the jets leave the rotating pipe. For the liquid jet, the exit angle ϕ_0 is given by

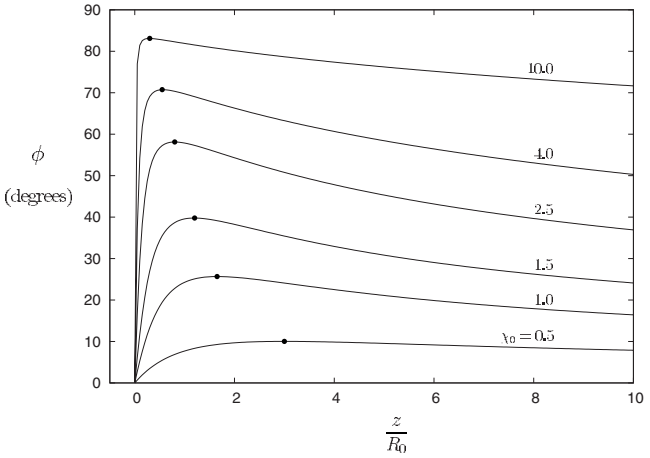

FIG. 8. Variation of the angle ϕ of granular jets with downstream coordinate z for selected values of χ_0 at $\mathrm{Fr}_0 = 1.0$. The local maximum angles $\phi_{\max}$, shown by the solid dots, tend to $\pi/2$ as χ_0 tends to infinity.

$$\tan\phi_0 = \left[\frac{dR(z)}{dz}\right]_{z=0} = -\frac{1}{2(\chi_0^2+2)\mathrm{Fr}_0}, \tag{29}$$

and the exit angle for the granular jet is

$$\tan\phi_0 = \left[\frac{dR(z)}{dz}\right]_{z=0} = \left[\frac{\chi_0^2}{R_0} z\right]_{z=0} = 0, \tag{30}$$

when the limit is taken holding χ_0^2/R_0 fixed. We see the interesting fact that all granular jets leave the rotating pipe with zero deflection from vertical, i.e., $\phi_0 = 0$ independent of χ_0. This mathematical feature may be seen in the sample profiles plotted in Fig. 4, but is not visible in Figs. 3 and 7 owing to the large horizontal scale used for these plots. The inward deflection ϕ_0 of the liquid jet, on the other hand, depends on both χ_0 and Fr_0 through Eq. (29); an increase in either the average exit velocity W_0 or pipe rotation Ω_0 causes a decrease in deflection angle. Moreover, the result in Eq. (29) reduces to $\tan\phi_0 = -(4\mathrm{Fr}_0)^{-1}$ for a stationary liquid jet $\chi_0 = 0$, in agreement with that obtained using Eq. (1).

To understand more clearly the implication of Eq. (30) for the granular jet, we note that if the limit $\chi_0 \to \infty$ was taken with $z = z_0$ small but finite, one would obtain $\phi_0 = \pi/2$. The variation of the granular jet angle $\phi(z)$ downstream of the exit is readily calculated from the analytic solution (23). This variation is displayed in Fig. 8 for selected values of χ_0 at $\mathrm{Fr}_0 = 1.0$. Note that the maxima (marked by solid dots) tend toward $\pi/2$ with increasing χ_0. Thus, although the angle of the granular jet is pinned to $\phi = \phi_0 = 0$ at the exit, it increases rapidly to a maximum value shortly downstream before it slowly decreases as gravity takes hold over particle centrifugation. In Fig. 9 we compare the χ_0-variation of these maximum jet angles for the granular jet with those for an inviscid liquid jet, also computed at $\mathrm{Fr}_0 = 1.0$. The initial angles are $\phi_0 = 0°$ for the granular jet and $\phi_0 = -14.04°$ for the liquid jet. The liquid jet angle rapidly approaches zero with increasing χ_0 and it is clear that the maximum angle of the granular jet tends asymptotically to 90° as $\chi_0 \to \infty$.

We now address the underpinning physics that distinguishes the shapes of these jets. For the rotating inviscid jet,

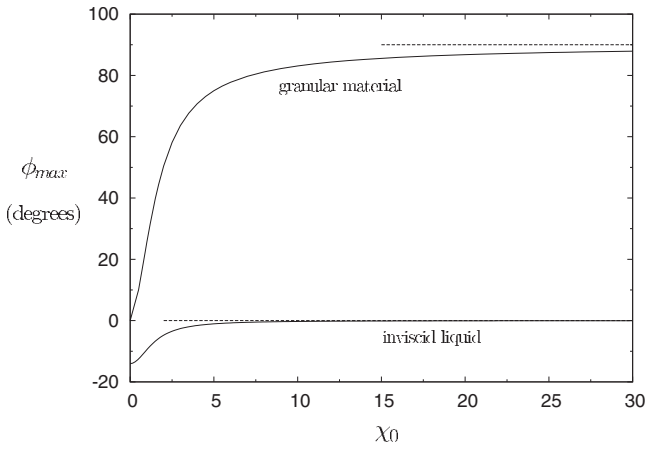

FIG. 9. Variation of maximum jet angles $\phi_{\max}$ with χ_0 for liquid and granular jets at $\mathrm{Fr}_0=1.0$. The exit angle of the granular jet is $\phi_0=0°$ while that for the inviscid liquid jet is $\phi_0=-14.04°$.

the resistance to jet contraction at large rotation rate is readily explained using the Taylor–Proudman theorem,[20] which states that at high Rossby number $\mathrm{Ro}\equiv\chi_0^{-1}$ away from rigid boundaries, vortex lines cannot be stretched; i.e., the flow is constrained to be independent of the vertical coordinate. Indeed, the liquid jet does not contract at all in the limit $\chi_0\rightarrow\infty$. The physics underlying the blossoming granular jet profiles is also simple: there is no surface tension to arrest the radial expansion centrifugally induced at the exit of the rotating pipe. Of interest here is the idea recently pointed out by Cheng *et al.*[19] that a noncohesive granular jet may, under certain circumstances, be conceptualized as a liquid with zero surface tension.

V. CONCLUSION

We have presented a new solution of the steady Bernoulli equation, under the slowly varying (slender jet) approximation in the absence of surface tension, for the shape of an inviscid rotating liquid jet shown to depend on two parameters: the exit Froude number Fr_0 and the exit swirl parameter χ_0. All rotating jet profiles displayed in Fig. 2 contract more slowly than the stationary jet for which $\chi_0=0$. Although this solution is derived using a minimal model, it clearly reveals the underlying physics of contraction for (stable) inviscid rotating liquid jets. The obvious sequel to the present investigation for future research would be a study that includes the primary neglected effect of viscosity.

We have further presented a simple theoretical model and taken experimental measurements for the shape of noncohesive granular jets discharged from a vertical pipe uniformly rotating at angular velocity Ω_0. There is no need for the slender jet approximation in this model which is predicated on the dynamics of noncolliding particles in the absence of air drag. In contrast to a rotating inviscid liquid jet, experiments show that at sufficiently high pipe rotation rate, a granular jet expands rather than contracts. Like the inviscid liquid jet, features of the granular free jet depend on Fr_0 and χ_0 only. Measurements of the variation of average exit speed W_0 for Ottawa sand as a function of pipe rotation rate Ω_0 in Fig. 5 reveal two regions of gradually decreasing velocity separated by a rather narrow transition from high discharge velocities (28 cm/s) in region I to very low discharge velocities (less than 0.3 cm/s) in region II. The flow is effectively continuous up to the end of the transition region ($\Omega\simeq 92$ rad/s) while it is characterized by sporadic particle ejections in region II. The measured profiles in Fig. 7 agree with theoretical prediction only at sufficiently high pipe rotation—at slower rotation rates the jet becomes more narrow and dense, so one cannot neglect the inelastic collsions among grains. The experiments allow us to infer that above $\Omega_1\simeq 20$ rad/s the particle flow is effectively collsion-free. The good agreement between experiment and theory above Ω_1 in region I suggests that the theoretical model is valid over the range $\Omega_1<\Omega_0<\Omega_2$, where $\Omega_2\simeq 75$ rad/s marks the beginning of the transition region for this experimental setup.

The granular flow dynamics within the pipe is much more complex than the external free jet flow, yet we have nonetheless endeavored to derive a criterion for the critical angular velocity Ω_c at which the particles adjacent to the wall of the pipe first become arrested. The obtained estimate $\Omega_c\simeq 77$ rad/s is very close to the value for onset of the transition region $\Omega_2\simeq 76$ rad/s found in our experiment. Clearly, the flow in the transition region is very complex, and it is surprising that our criterion for the onset of the transition region is so close to that experimentally observed. Certainly, the model may be criticized in various ways. For example, it is not presently known if the integrated centrifugal force and the static Janssen force acting normal to the cylindrical wall may be linearly superposed. Nevertheless, the order-of-magnitude agreement with observation suggests the model represents a reasonable first step toward understanding the difficult problem of gradual flow arrest in the transition region.

There are many possible extensions of this work that will likely improve our knowledge of the behavior of both internal and external granular flow under rotation. One could investigate flows emanating from rotating planar orifices, develop models and perform experiments using cohesive materials, and take into account the shear effect of the ambient gas. Studies along these lines are now in progress.

ACKNOWLEDGMENTS

Discussions with Francisco Higuera (ETSI Aeronáuticos, Madrid), Andrzej Herczynski (Boston College), and A. M. J. Davis (UC San Diego) on the subject of this study are greatly appreciated. The authors appreciate the assistance of Aaron Archundia for making careful repeat measurements of the granular jet profiles. One of us (A.M.) acknowledges COFFA and SIP, both from IPN, by fellowships given to participate in Project No. 20082903.

[1] J. Eggers and E. Villermaux, "Physics of liquid jets," Rep. Prog. Phys. **71**, 036601 (2008).
[2] S. P. Lin and R. D. Reitz, "Drop and spray formation from a liquid jet," Annu. Rev. Fluid Mech. **30**, 85 (1998).
[3] S. Middleman, *Modeling Axisymmetric Flow* (Academic, New York, 1995).
[4] J. P. Kubitschek and P. D. Weidman, "Helical instability of a rotating viscous liquid jet," Phys. Fluids **19**, 114108 (2007).

[5]J. P. Kubitschek, "The effect of viscosity on the stability of a uniformly rotating liquid column," Ph.D. thesis, University of Colorado, 2006.
[6]D. F. Rutland and G. J. Jameson, "Droplet production by the disintegration of rotating liquid jets," Chem. Eng. Sci. **25**, 1301 (1970).
[7]J. Eggers and M. P. Brenner, "Spinning jets," *IUTAM Symposium on Nonlinear Waves in Multi-Phase Flow*, edited by H.-C. Chang (Kluwer, Dordrecht, 2000), pp. 185–193.
[8]J. P. Kubitschek and P. D. Weidman, "The effect of viscosity on the stability of a uniformly rotating liquid column in zero gravity," J. Fluid Mech. **572**, 261 (2007).
[9]N. Savva and J. W. M. Bush, "The stability of rotating jets," Bull. Am. Phys. Soc. **49**, 53 (2004).
[10]R. L. Brown and J. C. Richards, *Principles of Powder Mechanics* (Pergamon, New York, 1970).
[11]J. Duran, *Sands, Powders, and Grains* (Springer, New York, 1999).
[12]K. Wieghardt, "Experiments in granular flow," Annu. Rev. Fluid Mech. **7**, 89 (1975).
[13]Y. Bertho, F. Giorgiutti-Dauphiné, T. Raafat, E. J. Hinch, H. J. Herrman, and J. P. Hulin, "Powder flow down a vertical pipe: The effect of air flow," J. Fluid Mech. **459**, 317 (2002).
[14]M. E. Möbius, "Clustering instability in a freely falling granular jet," Phys. Rev. E **74**, 051304 (2006).
[15]J. F. Boudet, Y. Amarouchene, B. Bonnier, and H. Kellay, "The granular jump," J. Fluid Mech. **572**, 413 (2007).
[16]H. A. Janssen, "Versuche über Getreidedruck in Silozellen," Z. Ver. Dtsch. Ing. **39**, 1045 (1895).
[17]Y. Bertho, F. Giorgiutti-Dauphiné, and J. P. Hulin, "Dynamical Janseen effect on granular packing with moving walls," Phys. Rev. Lett. **90**, 144301 (2003).
[18]C. Mankoc, A. Janda, R. Arévalo, J. M. Pastor, I. Zuriguel, A. Garcimartín, and D. Maza, "The flow rate of granular materials through an orifice," Granular Matter **9**, 407 (2007).
[19]X. Cheng, G. Varas, D. Citron, H. M. Jaeger, and S. R. Nagel, "Collective behavior in a granular jet: Emergence of a liquid with zero surface tension," Phys. Rev. Lett. **99**, 188001 (2007).
[20]H. P. Greenspan, *The Theory of Rotating Fluids* (Cambridge University Press, Cambridge, 1969).